

Article

Not peer-reviewed version

---

# Exploring the Fire Regime in Gilé National Park, in Zambezia Province, Central Mozambique

---

[J. C. Domingos](#) , F. Montfort , [S. N. Lisboa](#) , [V. Buramuge](#) , A. Senkoro , I. S. Maquia , [A. I. Ribeiro-Barros](#) , [N. S. Ribeiro](#) \*

Posted Date: 17 December 2025

doi: 10.20944/preprints202512.1429.v1

Keywords: fire intensity; fire density; fire frequency; fire risk; fire severity MODIS fire active; MODIS burned area



Preprints.org is a free multidisciplinary platform providing preprint service that is dedicated to making early versions of research outputs permanently available and citable. Preprints posted at Preprints.org appear in Web of Science, Crossref, Google Scholar, Scilit, Europe PMC.

Copyright: This open access article is published under a [Creative Commons CC BY 4.0 license](#), which permit the free download, distribution, and reuse, provided that the author and preprint are cited in any reuse.

Disclaimer/Publisher's Note: The statements, opinions, and data contained in all publications are solely those of the individual author(s) and contributor(s) and not of MDPI and/or the editor(s). MDPI and/or the editor(s) disclaim responsibility for any injury to people or property resulting from any ideas, methods, instructions, or products referred to in the content.

Article

# Exploring the Fire Regime in Gilé National Park, in Zambezia Province, Central Mozambique

J. C. Domingos <sup>1</sup>, F. Montfort <sup>2</sup>, S. N. Lisboa <sup>1,2</sup>, V. Buramuge <sup>1</sup>, A. Senkoro <sup>3</sup>, I. S. Maquia <sup>4</sup>, A. I. Ribeiro-Barros <sup>5</sup> and N. S. Ribeiro <sup>1,\*</sup>

<sup>1</sup> Departamento de Engenharia Florestal, Faculdade de Agronomia e Engenharia Florestal, Universidade Eduardo Mondlane Campus Universitario Principal, Building # 1, PO Box 257, Maputo, Mozambique

<sup>2</sup> N'Lab, Nitidæ, Montpellier, France

<sup>3</sup> Departamento de Ciências Biológicas, Universidade Eduardo Mondlane, CP 257, Maputo, Mozambique

<sup>4</sup> Centro de Biotecnologia, Universidade Eduardo Mondlane, CP 257, Maputo, Mozambique

<sup>5</sup> Universidade de Lisboa, Instituto Superior de Agronomia, Lab. Associado TERRA, Centro de Estudos Florestais, Portugal, Lisboa

\* Correspondence: joluci2000@yahoo.com

## Abstract

Miombo forest in Gilé National Park (PNAG), central Mozambique have significant habitat for endemic biodiversity but face mounting pressure from recurrent fire disturbance. This study assessed fire patterns and mapped fire risk in support of adaptive management in the PNAG. We investigated miombo fire regime over 23 years (2001 to 2023) in terms of return intervals, frequency, temporal distribution, spatial density and intensity, area extent, and severity, by using two MODIS satellite products (MCD14ML active fire; MCD64A1 burned area). Primary risk drivers were established and spatial fire likelihood mapped, using Random forest algorithm. Analysis revealed pronounced late dry-season burning (August-October) affecting approximately 60% of PNAG annually, especially in central-northern and eastern landscapes. Remarkably, 88% of the park maintain 1 to 2 year fire return interval while only 7% maintains return frequencies of 3 to 4 year cycles, important for maintaining Miombo ecosystem functionality. Medium to medium-high fire severity covered 98% of total fire areas. Climate-related drivers and hunting activities were identified as key fire imitators, peaking in central areas in terms of likelihood. Findings demonstrate urgent need for spatially-differentiated fire governance incorporating strategic zoning and prescribed burning to maintain PNAG's ecological resilience and conservation value.

**Keywords:** fire intensity; fire density; fire frequency; fire risk; fire severity MODIS fire active; MODIS burned area

## 1. Introduction

Spanning approximately 1.9 million km<sup>2</sup> across seven southern African nations including Angola, the Democratic Republic of Congo, Malawi, Mozambique, Tanzania, Zambia and Zimbabwe, Miombo woodlands constitute one of the largest ecosystem in this region in terms of geographical area coverage (Frost, 1996; Dziba et al., 2020). These forests fulfil critical ecological functions within the global climate system, including carbon storage and the regulation of fundamental biogeochemical processes (Frost, 1996; Ribeiro et al., 2020). In Mozambique, Miombo formations dominate the national forest landscape, accounting for approximately two-thirds of total forest cover (Aquino et al., 2018). The biological richness of this ecosystem is remarkable, hosting high levels of floristic and faunal diversity, including endemic and threatened taxa (Campbell et al., 1996; Dewees et al., 2011; Assédé et al., 2020).

The socioeconomic significance of Miombo woodland is equally substantial: over 70% of Mozambique's population relies directly on these forest resources, which contribute approximately

20% to household monetary income and 40% to non-monetary subsistence (Aquino et al., 2018; Magalhães, 2025).

Miombo ecological dynamics result from complex interactions among climatic factors, herbivory and human activities (Ribeiro et al., 2013, 2020), with fire serving as a cross-cutting element influencing all these process (Boramuge et al., 2023). Fires has been a historic and structuring component of this ecosystem, shaping floristic diversity, regeneration patterns, and vegetation succession, while also promoting ecological processes such as seed germination and soil nitrification (Furley et al., 2008).

However, departures from historical burning patterns pose growing threats to ecosystem integrity (Aragão et al., 2008). Shifts in fire regime can trigger significant negative impacts, including soil degradation, biodiversity loss, and structural transformations within the ecosystem (Frost & Robertson, 1987; Ribeiro et al., 2008, 2013; Meneses et al. 2024; Salimo et al. 2025). Such alterations consequently undermine the ecosystem's capacity to deliver goods and services to rural and urban communities dependent on Miombo resources (Miombo Network, 2016).

Fire regime encompasses the temporal and spatial patterns of burning within a given area (Whitlock et al., 2010), incorporating components such as seasonality, extent, return interval, intensity, severity, and risk (Krebs et al., 2010; Whitlock et al., 2010). Two components are particularly critical for understanding fire ecology (Keeley, 2009): Burning frequency—the temporal interval between consecutive fire events—determines the recovery period available for vegetation to restore pre-fire characteristics before the next occurrence (Gandiwa, 2011); Fire intensity—the energy released during combustion—combined with severity, defines the magnitude of potential ecosystem impacts, such as adult tree mortality, suppression of natural regeneration, and faunal decline (Frost, 1996).

The study of burning frequency and intensity is fundamental to understanding fire-ecosystem relationships, particularly under global climate change scenarios (Pausas and Keeley, 2009). Within Miombo woodlands, where fire has a long coexistence history with vegetation, multiple authors have established that a 3–4 year return interval represents a functional threshold (Frost, 1996; Govender et al., 2006; Macave et al., 2022; Salimo et al., 2025). This pattern promotes biodiversity maintenance, nutrient cycling, and prevention of catastrophic fires, thereby ensuring ecosystem health and resilience.

Fire risk expresses the probability of fire occurrence as a function of multiple factors: fuel load, climatic conditions, vegetation cover type, topography, and anthropogenic activities (Koproski et al., 2011; Torres et al., 2011; Vallejo-Villalta *et al.*, 2019). Consequently, susceptibility mapping becomes essential for identifying fire-prone areas, enabling targeted investments in monitoring and adaptive management strategies (Frost, 1996; Ryan et al., 2016; Novo et al., 2020).

Currently, several remote sensing platforms are available for fire mapping and monitoring, with technology selection depending on specific study objectives and area characteristics (Chuvienco et al., 2019). The Moderate Resolution Imaging Spectroradiometer (MODIS) has transformed fire monitoring in Miombo woodlands, enabling detailed multi-year fire regime analyses in Mozambique and the region (Ribeiro et al., 2007; Silva et al., 2005; Archibald et al., 2009; Boramuge et al., 2023; Meneses et al., 2024, 2025). This technology has proven particularly valuable for understanding fire dynamics and implementing adaptive management strategies (Archibald et al., 2009; Ryan et al., 2016).

MODIS's primary advantage lies in providing consistent and continuous data over decades, with standardized algorithms facilitating extensive temporal analyses and inter-annual comparisons—fundamental aspects for fire regime characterization (Giglio et al., 2013; Andela et al., 2017).

Understanding fire regimes assumes particular relevance in protected areas, which serve as biodiversity conservation strongholds. Gilé National Park (PNAG), located in central Mozambique, constitutes a priority conservation area where fires are identified as a primary cause of forest degradation and a management priority (ANAC, 2024).

However, significant research gaps exist regarding fire regimes and risk in this area, limiting evidence-based decision-making. This work represents one of the first multi-year (2001–2023) analyses to characterize and map fire regime and risk in PNAG, aiming to inform fire management in the park. Globally, this study contributes to ongoing debates about fire occurrence and impacts under climate change. Our Specific Objectives: (i) To determine fire frequency, seasonality, density, and intensity during 2001–2023; (ii) To determine and map the spatial distribution of fire severity; (iii) To model the main determinants of fire risk in PNAG.

## 2. Materials and Methods

### 2.1. Study Area

Our research was carried out in Gilé National Park (PNAG), situated in Zambezia Province, central Mozambique, encompassing portions of Gilé and Pebane Districts in the province's northeastern sector. The park spans 4,532 km<sup>2</sup>, comprising a 2,861 km<sup>2</sup> core protection zone and a 1,671 km<sup>2</sup> buffer zone. Three major watercourses characterize the park's hydrology: the Mulela River delineates the western boundary, the Molocué River defines the eastern perimeter, while the Malema River represents the primary drainage system within the park's interior. Additional permanent watercourses include the Naivocone River in the northern sector, the Nakololo, Malemacuculo, and Mucussa Rivers within the core area, and the Muipige and Enrorue Rivers in the southern portion (ANAC, 2024). The area's conservation status evolved from its initial establishment as a game reserve in 1932, through designation as a National Reserve in 1999 (Mercier et al., 2016), to its current status as a National Park under Decree 44/2020 of June 17, 2020 (ANAC, 2024). Park management infrastructure includes seven ranger outposts and an administrative center located at Musseia (Figure 1).

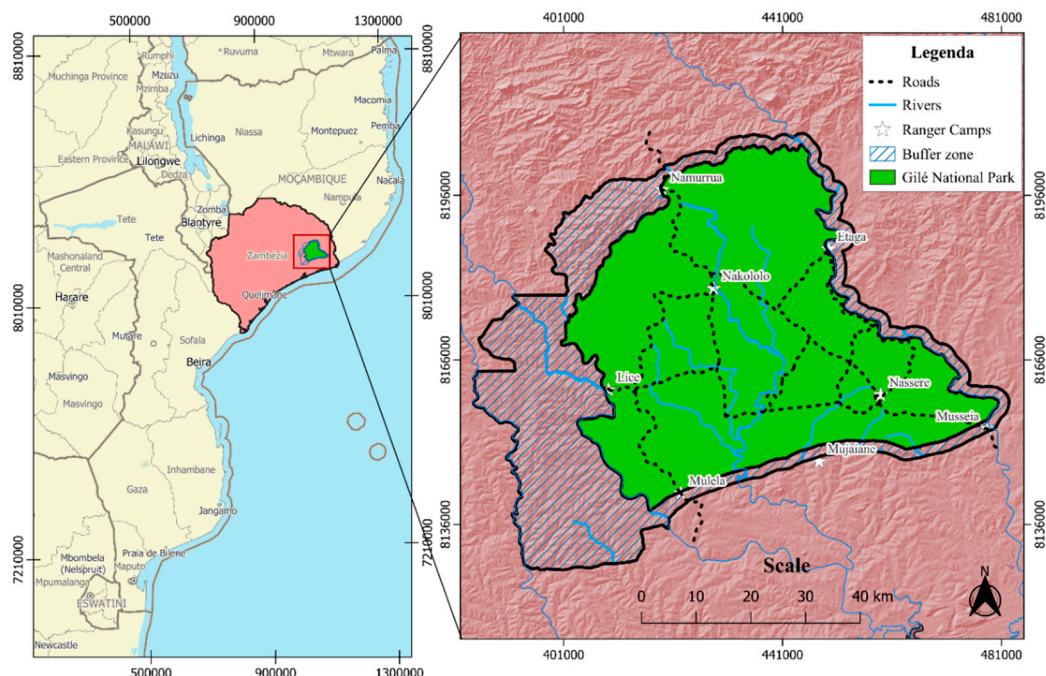


**Figure 1.** Geographic location map of Gilé National Park, Zambezia Province, Central Mozambique. Background image: ESRI Shaded Relief.

Plains dominate the park's topography, with mean elevations around 160 m above sea level, while northern mountainous areas attain maximum elevations of 1,052 m (Montfort et al., 2021). According to Köppen classification, the climate is tropical savanna, featuring distinct wet (November–April) and dry (May–October) seasons, with mean annual precipitation of 1,296 mm and

temperatures ranging between 20 °C and 31 °C during 2010–2020 (Huntington et al., 2017). Miombo woodlands constitute the dominant vegetation type across PNAG, recognized as among Mozambique’s most biodiverse and ecologically intact landscapes (ANAC, 2024). Characteristic Miombo flora documented in the park includes *Brachystegia spiciformis* Benth., *B. boehmii* Taub., *Julbernardia globiflora* (Benth.) Troupin, *Diplorhynchus condylocarpon* (Müll.Arg.) Pichon, *Millettia stuhlmannii* Taub., and *Parinari curatellifolia* Planch. ex Benth., among others (Pungulanhe, 2020).

Approximately 12,000 people inhabit the buffer zone (Etc Terra, 2017), depending on natural resource extraction for livelihood sustenance through activities such as shifting cultivation, apiculture, wildlife harvesting, and non-timber forest product collection (Mercier et al., 2016). Consequently, the buffer zone presents a heterogeneous landscape mosaic comprising Miombo regeneration of varying ages, agricultural plots (mango, cashew, maize, cassava, legumes, groundnuts), mature woodland stands, and wooded savannas (Montfort et al., 2021; Ameja et al., 2022). Fire application is prevalent across these land-use activities.

## 2.2. Data Acquisition

### 2.2.1. Fire Data

Our analysis utilized two MODIS Collection 6 fire products spanning January 2001 through December 2023: the daily 1-km active fire product (MCD14ML) and the monthly 500-m burned area product (MCD64A1). Active fire data were obtained via NASA’s Fire Information for Resource Management System (FIRMS; <https://firms.modaps.eosdis.nasa.gov/map/>), while burned area data were downloaded from the USGS LP DAAC data repository (<https://lpdaac.usgs.gov/tools/data-pool/>) in Hierarchical Data Format (HDF). To minimize false detections, we excluded active fire pixels below 30% confidence following recommendations for MODIS Collection 6 data (Giglio et al., 2018). This threshold differs from earlier Collection 5 analyses that typically employed  $\geq 70\%$  confidence filters (Giglio et al., 2003; Roy et al., 2008; Schroeder et al., 2008), reflecting algorithmic improvements in Collection 6 that enable reliable fire detection at lower confidence levels. For burned area analysis, we reclassified MCD64A1 pixel values originally encoded as 0 (unburned) or 1–366 (Julian burn day)—into binary format where 1 indicates burned and 0 indicates unburned conditions, using QGIS v3.34.7 (QGIS Development Team, 2024). Annual binary burn maps (n=23) were then aggregated to derive multi-year fire frequency surfaces.

### 2.2.2. Environmental and Socio-Economic Data

In this study, we investigated the role of several environmental and socio-economic factors in explaining the fire occurrence in the PNAG (Table 1).

**Table 1.** Details of the environmental and socio-economic variables used for modelling historical fire risk in Gile National Park.

Type	Variable name	Definition	Data source	Spatial resolution
Terrain	Altitude	Altitude (meters)	SRTM ( <a href="https://www.diva-gis.org/gdata">https://www.diva-gis.org/gdata</a> )	30 m
Terrain	Slope	Slope (degrees)	SRTM ( <a href="https://www.diva-gis.org/gdata">https://www.diva-gis.org/gdata</a> )	30 m
Terrain	Appearance	Tilt direction (degrees)	SRTM ( <a href="https://www.diva-gis.org/gdata">https://www.diva-gis.org/gdata</a> )	30 m
Land cover	LULC	Land use and occupation	Montfort, 2021	30 m

<b>Ground cover</b>	AGB BGB woody biomass	Above and below ground woody biomass (t/ha)	Montfort, 2021	30 m
<b>Ground cover</b>	NDVI	Normalized Difference Vegetation Index	MOD13Q1 ( <a href="https://code.earthengine.google.com/293acc173d3da3ebcebb2e58155ff99a">https://code.earthengine.google.com/293acc173d3da3ebcebb2e58155ff99a</a> )	250 m
<b>Ground cover</b>	NDVI anomalies	Normalized Difference Vegetation Index Anomalies	MOD13Q1 ( <a href="https://code.earthengine.google.com/293acc173d3da3ebcebb2e58155ff99a">https://code.earthengine.google.com/293acc173d3da3ebcebb2e58155ff99a</a> )	250 m
<b>Climate</b>	Precipitation	Annual precipitation (mm/year)	CHIRPS ( <a href="https://data.chc.ucsb.edu/products/CHIRPS/v3.0/">https://data.chc.ucsb.edu/products/CHIRPS/v3.0/</a> )	5000 m
<b>Climate</b>	Temperature	Temperature (degrees Celsius)	MOD11A2 ( <a href="https://landsweb.modaps.eosdis.nasa.gov/archive/allData/61/MOD11A2/">https://landsweb.modaps.eosdis.nasa.gov/archive/allData/61/MOD11A2/</a> )	1000 m
<b>Climate</b>	ET	Evapotranspiration potential	MOD16A2 Running et al., 2017	500 m
<b>Climate</b>	Wind	Wind speed (meters per second)	Worldclim ( <a href="http://www.worldclim.org">http://www.worldclim.org</a> )	1000 m
<b>Climate</b>	Water vapor pressure	Water vapor pressure (kPa)	Worldclim ( <a href="http://www.worldclim.org">http://www.worldclim.org</a> )	1000 m
<b>Climate</b>	Solar radiation	Solar radiation (kJ m <sup>-2</sup> day <sup>-1</sup> )	Worldclim ( <a href="http://www.worldclim.org">http://www.worldclim.org</a> )	1000 m
<b>Accessibility</b>	Villages	Euclidean distance from villages (meters)	INE	250 m
<b>Accessibility</b>	Roads	Euclidean distance from roads (meters)	Open Street Map (Montfort, 2021)	250 m
<b>Accessibility</b>	Rivers	Euclidean distance from rivers (meters)	FAO, WORLD BANK	250 m
<b>Accessibility</b>	Agriculture	Euclidean distance from agricultural fields (meters)	CENACARTA	30 m
<b>Demography</b>	Population	Population density (people/km <sup>2</sup> )	(Tiecke et al., 2017)	30 m
<b>Hunting</b>	Hunting Traps	Trap density (trap/km <sup>2</sup> )	PNAG	30 m

### 2.3. Data Pre-Processing and Analysis

#### 2.3.1. Pre-Processing

Prior to analysis, we standardized all spatial datasets by clipping to park boundaries and reprojecting to UTM Zone 37S (WGS 84 datum) using QGIS v3.34.7 reprojection tools (QGIS Development Team, 2024). To ensure spatial consistency, all raster layers described in Table 1 were resampled to 30-m resolution using the `projectRaster` function from the `raster` package in R v4.4.0 (R Core Team, 2023). No additional preprocessing was applied to MCD14ML data, as Collection 6 products undergo automated correction during operational processing including cloud masking, contextual fire pixel identification, and background characterization prior to distribution (Giglio et al., 2016, 2018). To standardise the representation of the data, all raster datasets described in Table 1

were adjusted to the same spatial resolution of 30 m, using the `projectRaster` function of the raster package of the R software version 4.4.0 (R Core Team, 2023).

### 2.3.2. Fire Frequency and Mean Fire Return Interval

We characterized fire regime components following established protocols (Ribeiro et al. 2017; Meneses et al. 2024). Fire frequency quantifies how many times fire affected each pixel during our 23-year study period, whereas mean fire return interval represents the average temporal spacing between successive burns at individual pixel locations (Bond & Keeley, 2005; He et al., 2019).

$$FF = \frac{1}{MFRI} \quad (1)$$

where: MFRI: Mean Fire Return Interval

$$MFRI = T * \frac{A}{a} \quad (2)$$

where T = total study period (23 years), A = total park area, and a = area burned within the study period.

The FF classes were defined taking as reference the MFRI threshold in Miombo of 3-4 years (Frost, 1996). Pixels within that range were defined as the “Medium FF class” and the other classes were generated for return intervals below (low FF class) and above (high FF class) that threshold. This resulted in 6 FF classes: (i) 0: no burn; (ii) 1–2: Low; (iii) 3–4: Medium (reference class); (iv) 5–10: Medium to high; (v) 10–18: High; and (vi) > 18: Very high (annual burning). The FF map was generated in QGIS Development Team (2024) version 3.40.7 by adding the annual area burned using the raster calculation tool.

### 2.3.3. Fire Seasonality

Temporal fire patterns were characterized by analyzing monthly distribution of active fire detections and burned area extent throughout the year. We extracted burn dates (Julian day format) from both MCD14ML active fire and MCD64A1 burned area products, then aggregated fire occurrences by calendar month across the entire study period (2001–2023). Following regional fire phenology classifications (Ribeiro et al., 2017), we categorized fire activity into three distinct seasons aligned with regional precipitation patterns: wet season (November–April), early dry season (May–July), and late dry season (August–October). This seasonal stratification enabled assessment of intra-annual fire variability and identification of peak burning periods. Monthly fire frequency and burned area were visualized through temporal distribution graphs to illustrate seasonal trends.

### 2.3.4. Extent of Burned Area and Fire Density

Cumulative burned area over the study period was quantified by summing annual binary burn maps in QGIS v3.40.7 (QGIS Development Team, 2024). Fire density—expressing the spatial concentration of fire detections—was calculated as:

$$Density = \frac{Number\ of\ active\ fires}{Total\ area\ (km - 2)} \quad (3)$$

Spatial patterns of fire density were visualized using kernel density estimation in QGIS v3.40.7, producing continuous surfaces depicting fire hotspots throughout the park.

### 2.3.5. Fire Intensity

Fire intensity was assessed using Fire Radiative Power (FRP) values embedded in MCD14ML data. FRP quantifies the instantaneous rate of radiative energy emission from active fires across all wavelengths and view angles, expressed in megawatts (MW) (Wooster et al., 2005; Silva Junior et al., 2018). This metric serves as a proxy for fire intensity—the heat release rate per unit time (Goryl et al., 2012).

We analyzed 25,119 fire detections occurring June–December during 2001–2023. Spatial clustering of fire intensity was identified through Getis–Ord  $G_i^*$  hotspot analysis in QGIS v3.34.7, which identifies statistically significant ( $p < 0.05$ ) spatial clusters of high FRP values (hot zones) versus low FRP values (cold zones). Areas exhibiting 95% and 99% statistical significance were classified as high-intensity fire zones. Continuous intensity surfaces were generated via Inverse Distance Weighting (IDW) interpolation of FRP values, producing spatially explicit fire intensity maps.

### 2.3.6. Fire Severity

Fire severity—reflecting ecological impact and ecosystem damage—was assessed using remotely sensed burn severity indices. We employed a Google Earth Engine (GEE) script adapted from UN-SPIDER recommended practices for burn severity assessment (UN-SPIDER, 2023) to process Landsat imagery from 2014–2023. The Normalized Burn Ratio (NBR) was computed from Landsat surface reflectance data following standard protocols (Lutes et al., 2006):

$$\text{NBR} = \frac{\text{NIR} - \text{SWIR}}{\text{NIR} + \text{SWIR}} \quad (4)$$

where NIR represents near-infrared reflectance and SWIR represents shortwave infrared reflectance.

Burn severity was quantified through the differenced Normalized Burn Ratio (dNBR), calculated by subtracting post-fire NBR from pre-fire NBR (Konkathi & Shetty, 2021).

$$\text{dNBR} = \text{NBR} (\text{prefire}) - \text{NBR} (\text{postfire}) \quad (5)$$

This metric captures fire-induced vegetation change, with higher dNBR values indicating greater severity. We classified dNBR values into severity categories following Key & Benson (2006): unburned/regenerating ( $\leq 0.099$ ), low (0.10–0.26), moderate (0.27–0.43), moderate-high (0.44–0.65), and high ( $> 0.66$ ) severity. Multi-year severity patterns were synthesized by aggregating annual severity maps in QGIS v3.40.7.

### 2.3.7. Fire Risk Mapping

We modelled fire occurrence probability using historical active fire locations as response variables and environmental/anthropogenic factors as predictors. To ensure data quality, fire detections underwent two-stage quality control: (1) exclusion of detections below 30% confidence, and (2) removal of statistically non-significant detections identified through hotspot analysis. Only high-confidence ( $> 95\%$  significance) detections were retained. From filtered detections, we generated a fire density surface using Inverse Distance Weighting (IDW) in QGIS v3.40.7, subsequently reclassified into binary format (0 = no fire/low density; 1 = fire/high density) to serve as the response variable.

Our modelling dataset comprised 5,362 locations: 2,681 historical fire occurrences paired with 2,681 randomly sampled non-fire locations generated in QGIS v3.40.7 (QGIS Development Team, 2024). The dataset was partitioned into 70% calibration and 30% validation subsets through random stratified sampling. Twenty explanatory variables spanning six thematic categories (Table 1) were extracted to each point location: terrain characteristics (elevation, slope, aspect), land cover (land use, aboveground biomass), vegetation indices (NDVI, NDVI anomalies), climate (precipitation, temperature, evapotranspiration, wind, vapor pressure, solar radiation), accessibility (distances to villages, roads, rivers, agriculture), demographics (population density), and anthropogenic pressure (hunting trap density).

Fire occurrence probability was modelled using Random Forest machine learning (Breiman, 2001), implemented through the randomForest package in R (Liaw & Wiener, 2002). This ensemble approach constructs multiple decision trees, each trained on bootstrap samples, with predictions aggregated across all trees to produce robust probability estimates (Montfort, 2021; Milà et al., 2024).

The calibrated model was applied across the study area to generate a continuous probability surface ranging from 0 (low fire risk) to 1 (high fire risk). For operational interpretation, this surface was reclassified into binary risk categories (0 = no/low risk; 1 = moderate-high risk).

Variable importance was assessed via Mean Decrease in Gini impurity (MDG), which quantifies each predictor's contribution to improving classification purity across decision tree nodes, averaged across the entire forest (Silva et al., 2019; Gonçalves et al., 2022). This metric identifies the most influential drivers of fire occurrence.

All spatial analyses and modelling were conducted in R v4.4.0 (R Core Team, 2023) using the randomForest package for model development (Liaw & Wiener, 2002) and the raster package for spatial data handling (Hijmans, 2025).

#### 2.4. Annual Burning Map Accuracy

Validation of fire frequency mapping incorporated field observations collected during 2022–2023 across 29 sampling plots (0.1 ha each; 50×20 m dimensions) distributed throughout the park. Field indicators included direct fire evidence, tree fire scars, mortality patterns, bark damage, and other burn signatures. For years 2001–2021, we used Google Earth imagery as validation reference data. Classification accuracy was evaluated through confusion matrix analysis, comparing mapped burn classifications against reference data (field observations and Google Earth imagery). We computed two accuracy metrics:

$$K = \frac{P_o - P_e}{1 - P_e} \quad (6)$$

where  $P_o$  represents observed agreement proportion (correctly classified pixels/total assessed pixels) and  $P_e$  represents expected agreement by chance (product of row and column marginals for each class).

Overall Accuracy: Calculated as the sum of correctly classified pixels (main diagonal) divided by total sample size.

### 3. Results

#### 3.1. Fire Regime

##### 3.1.1. Mean Fire Return Interval in the PNAG

Our 23-year analysis (2001-2023) revealed substantial variation in fire frequency across PNAG, ranging from completely fire-free pixels to those experiencing up to 24 fire events, averaging a rate of 0.26 fires annually per unit area. Spatial patterns (Figure 2) demonstrated pronounced fire frequency concentrated in the park's core region, with particularly elevated values surrounding the Lice, Nakololo, and Nassere ranger camps. Remarkably, fire touched nearly the entire landscape during our study timeframe, with merely 0.17% escaping combustion. The majority of PNAG (61.46%) experienced 11-18 burning episodes, classified as high frequency, while 14.44% endured 18 or more events (very high frequency). Collectively, high and very high frequency regimes characterized approximately three-quarters of the formally protected zone.

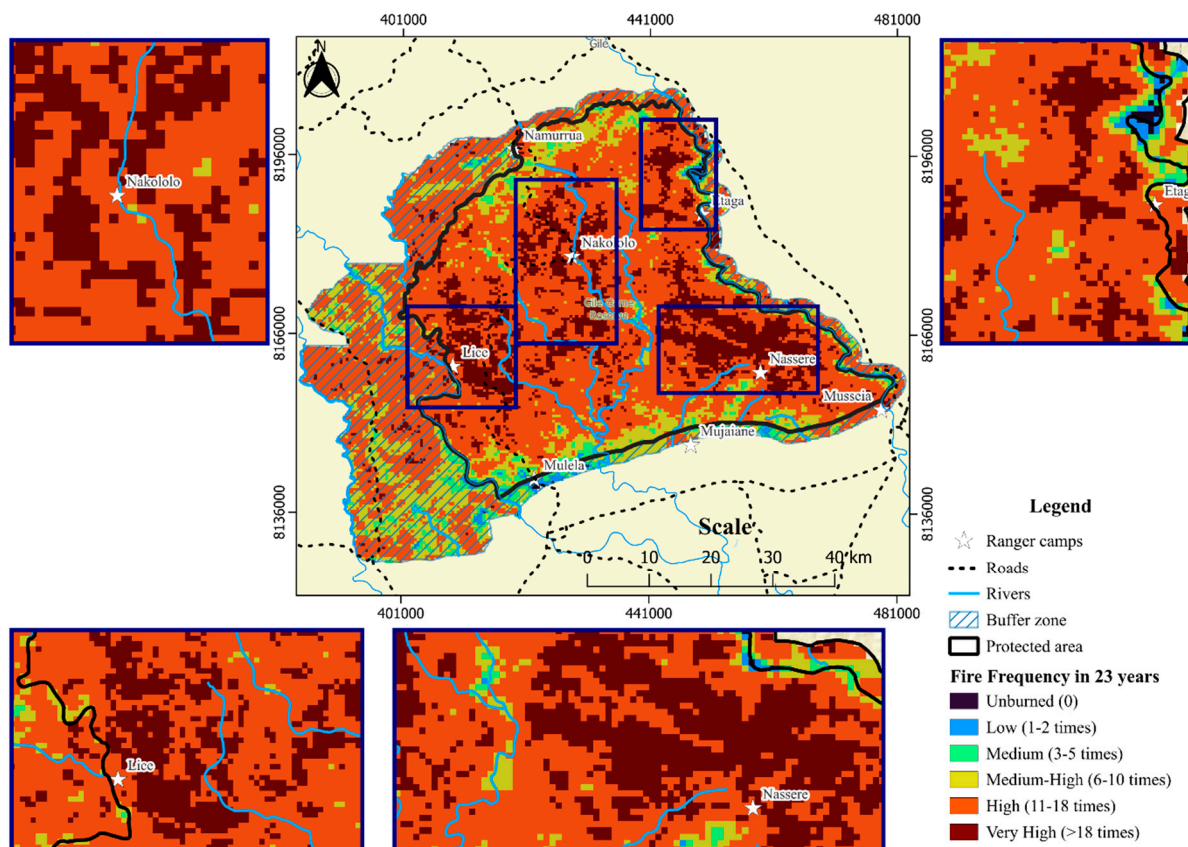


**Figure 2.** Spatial distribution of burning frequency over 23 years (2001-2023), in the Gilé National Park. Then insets represent FF in the vicinity of the main ranger camps inside the park.

Our calculations yielded an MFRI of 3.9 years, suggesting a typical recurrence cycle of approximately four years between successive fire events at any given location. However, this aggregate metric masks significant heterogeneity: as presented in Table 3, the vast majority (88%) experienced 1-2 year MFRI, whereas a negligible fraction (0.003%) persisted without fire throughout the entire observation period.

**Table 3.** Burned area by Mean fire return interval (MFRI) class.

MFRI class	Burned area (km <sup>2</sup> )	Burned area (%)
0	0.25	0.003
1-2	3863.01	88.46
3-4	314.05	7.19
5-8	101.10	2.32
9-12	29.84	0.68
13-23	16.53	0.38
N/A (No data/No fire)	42.27	0.97
Total	4,367	100

### 3.1.2. Fire Temporal Variation and Seasonality

Fire activity over the 23-year observation window affected approximately 99% of PNAG's 4,367 km<sup>2</sup> extent, indicating near-complete landscape involvement. Temporal analysis identified distinct peak years—2001, 2005, 2010, 2013, and 2023—when burned area extent reached maximum values. Among these, 2010 emerged as the most extreme fire year, expanding roughly 80% of PNAG including the buffer zone. Conversely, 2003 represented the minimum extent, with combustion

limited to approximately 43% of the landscape (including buffer areas) (Figure 3). Fires occur mainly during the late-dry season, between August and October (Figure 3)

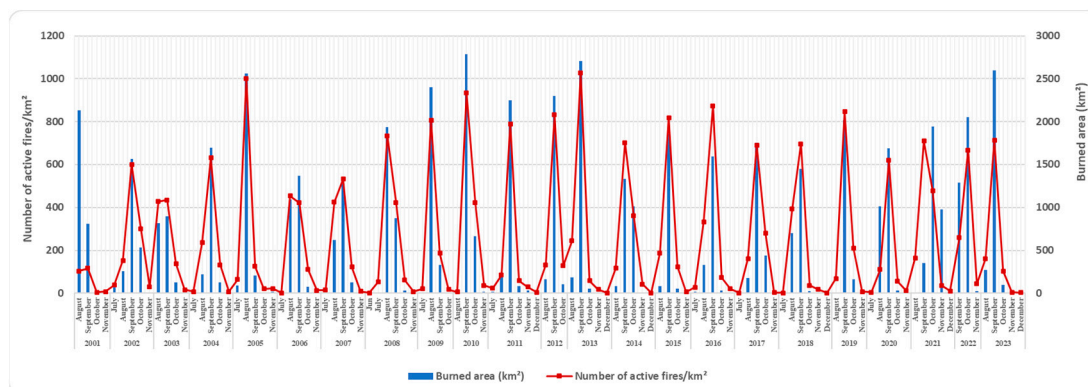


**Figure 3.** Intra-annual and inter-annual distribution of fire outbreaks and the extent of the burned area during the period between 2001 and 2023 in the Gilé National Park, Central Mozambique.

### 3.1.3. Fire Intensity and Density

Fire Radiative Power measurements across the study period averaged 36.24 MW, spanning a range from 5.75 MW (August 2015 minimum) to 858.63 MW (September 2021 maximum). High and very high intensity categories collectively characterized roughly one-third (35%) of PNAG's landscape (Table 4, Figure 4).

**Table 4.** Area covered by each fire intensity class.

Intensity (Megawatts)	Area (km <sup>2</sup> )	% of the total park area
N/A (No data/No fire)	1.66	0
Low (5.37-18.75)	637.53	15
Medium (18.76–25.45)	961.86	22
Medium to High (25.46–35.48)	1201.92	28
High (35.49-48.87)	844.25	19
Very High (>48.88)	719.78	16
Total	4,367	100

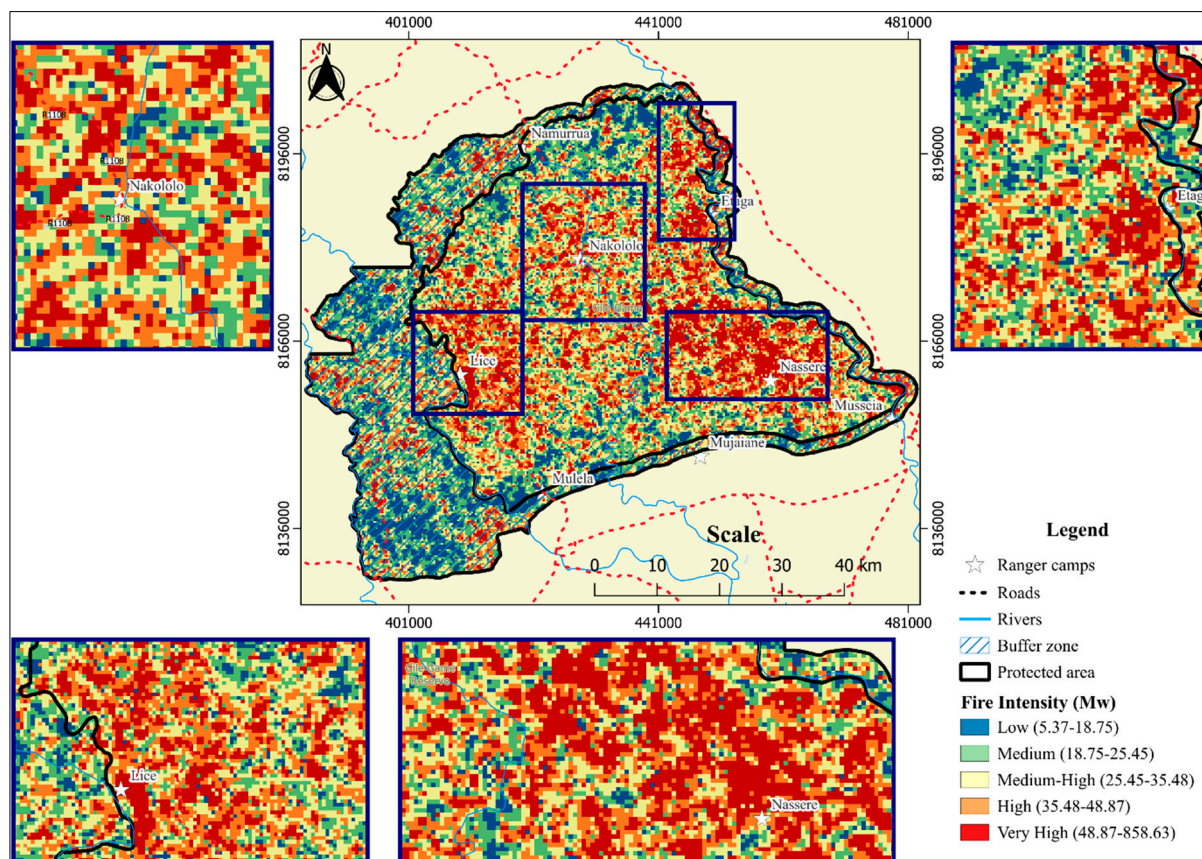


**Figure 4.** Spatial distribution of burning intensity over 23 years (2001-2023), in the Gilé National Park. The insets represent the density of fire in the vicinity of the ranger camps.

Spatial fire occurrence density averaged 206 ignitions  $\text{km}^{-2}$  over the observation period (Table 5, Figure 5), with values ranging from 14.86 to 859.92 fires  $\text{km}^{-2}$  (September 2015 maximum). Low density fire regimes (14.86-114.27 ignitions  $\text{km}^{-2}$ ) occupied merely 18% of PNAG's total extent, predominantly within buffer zones in the southern and southwestern sectors, as well as near the Namurrua ranger camp (Table 4). About 20.47% of the total area of the PNAG had medium-density fires ranging from 114.28 to 163.98 fires per  $\text{km}^2$ . Approximately 60.59% of the park's total area was dominated by medium—to very high-density fires, which were more concentrated in the park's total protection zone (Figure 5).

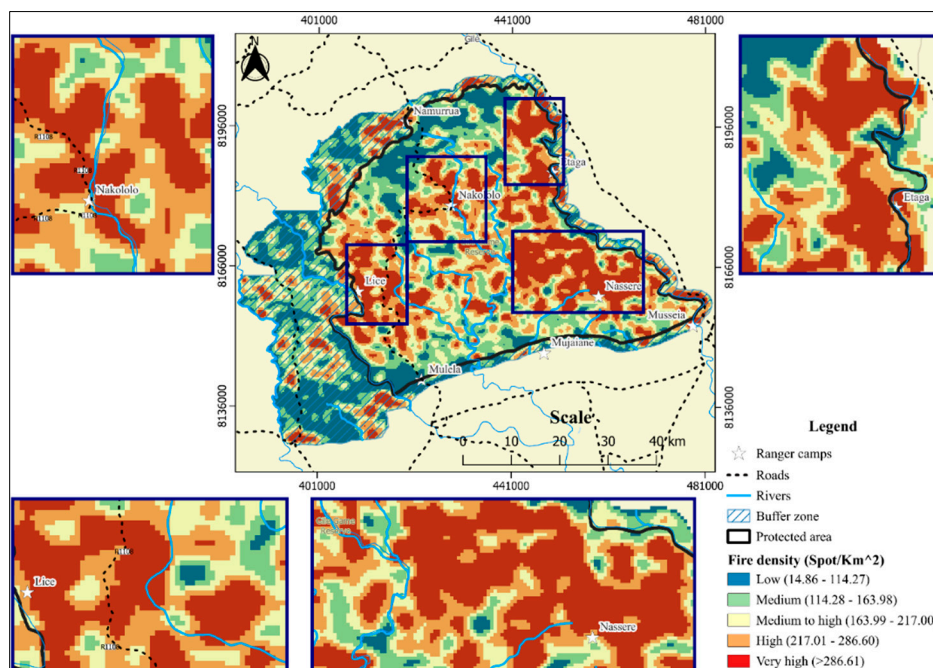


**Figure 5.** Spatial distribution of burning density over 23 years (2001-2023), in the Gilé National Park. The inset represents the density of fires in the vicinity of the ranger camps.

**Table 5.** Area occupied by each class of fire density in the Gilé National Park.

Density (Fires/km <sup>2</sup> )	Area (km <sup>2</sup> )	%
N/A (No data/No fire)	14.14	0.33%
Low (14.86 -114.27)	812.91	18.61%
Medium (114.28-163.98)	894.14	20.47%
Medium to High (163.99–217.00)	891.11	20.41%
High (217.01 -286.60)	890.49	20.39%
Very High (>286.60)	864.22	19.79%
Total	4367	100

### 3.1.4. Fire Severity

dNBR analysis revealed that medium to medium-high severity burns dominated PNAG, affecting 98% of the landscape (Figure 6, Table 6). High severity fires remained exceedingly rare, encompassing just 0.04% of the park. Unlike frequency and intensity patterns, severity distribution exhibited no discernible spatial structure.

**Table 6.** Fire Severity in Gilé National Park. dNBR is the difference in Normalized Burned Ratio.

Fire Severity	Area (km <sup>2</sup> )	%
Unburned/Regeneration (dNBR>0.099)	6.95	0.16%
Low severity (dNBR: 0.1–0.26)	51.13	1.17%
Medium severity (dNBR: 0.27–0.43)	2,463.47	56.41%
Medium to high severity (dNBR: 0.44-0.65)	1,832.62	41.97%
High severity (dNBR>0.66)	1.53	0.04%
N/A (No data/no fire)	11.30	0.26%
Total	4367	100%

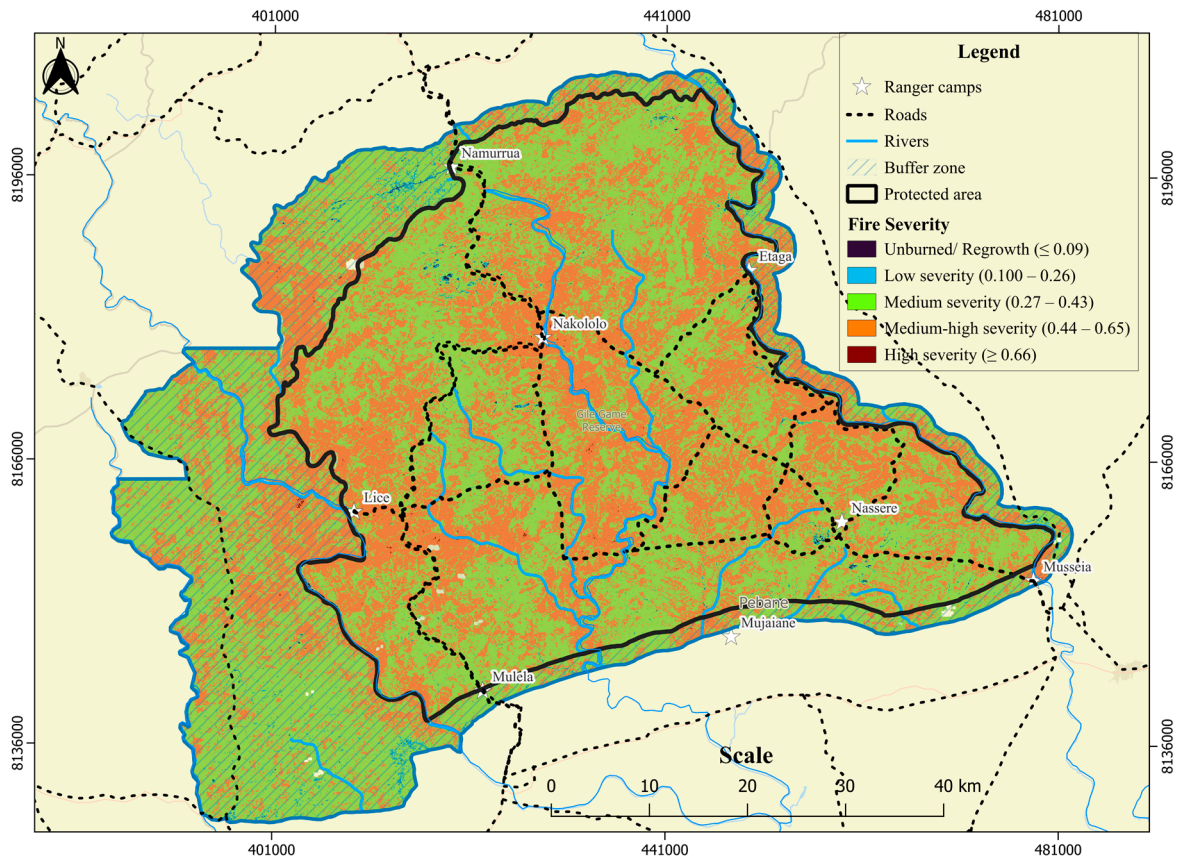


**Figure 6.** Fire severity map in Gilé National Park, central Mozambique. Fire severity is given by the dNBR (difference Normalized Burned Index).

### 3.2. Fire Risk Mapping

#### 3.2.1. Fire Risk Factors

Based on the MDG scores, eight variables with highest importance were selected from the 20 used to train our model: precipitation, solar radiation, water vapor pressure, distance to access roads, distance to agricultural lands, wind speed, distance to villages, and hunting trap density (Figure 7).

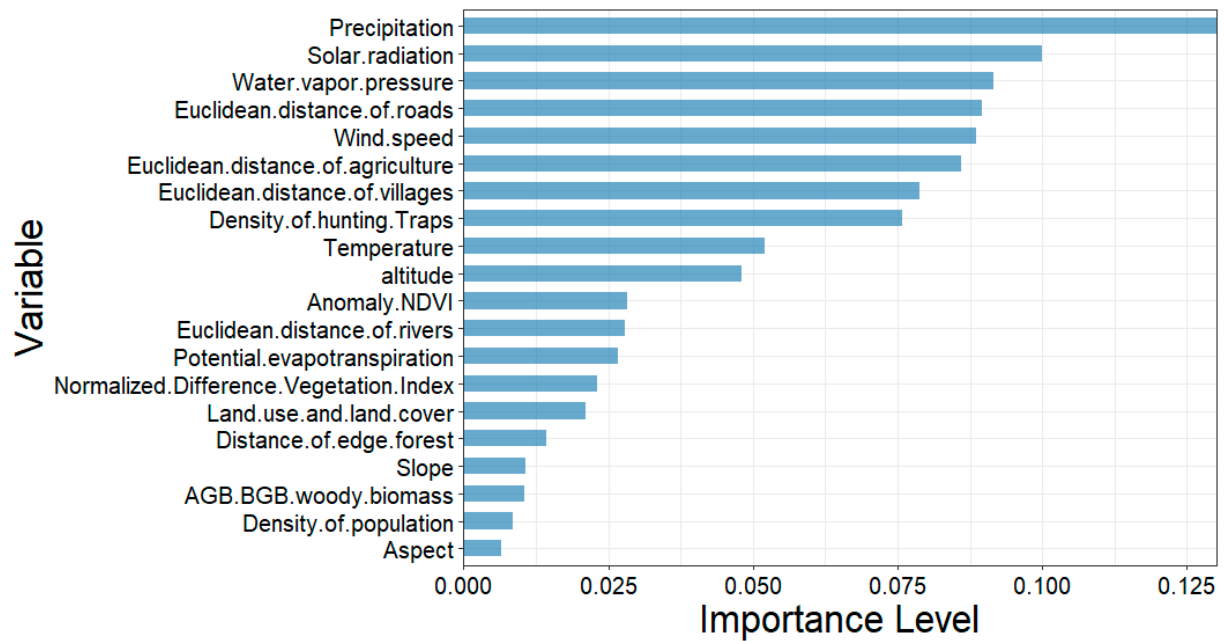


**Figure 7.** Importance of the fire predicting variables according to the Mean decrease Gini index.

Figure 8 shows the partial dependence of the first eight most important variables selected using the Random Forests algorithm. The results show that precipitation below the range of 1,150 to 1,200 mm increased fire ignition probability and the risk decreased when it exceeded 1,200 mm. Solar radiation influenced the ignition of fires from 17,800kJ/day onwards. Areas closer to the villages presented a lower risk of fires, whereas areas more than 15,000m away had a greater fire risk. Agricultural activity influenced the ignition of fires when they were within 10,000 to 20,000 meters, and the risk decreased when the distance was above 20,000 meters. The distance to roads influenced the ignition of fires when they were 10,000 meters away. However, at zero (0) meters away, there was a very low probability of fires both in areas near agricultural lands and on access roads. Regarding the density of hunting traps, they showed that above 0.2 traps/km<sup>2</sup> there was a greater probability of fire risk.

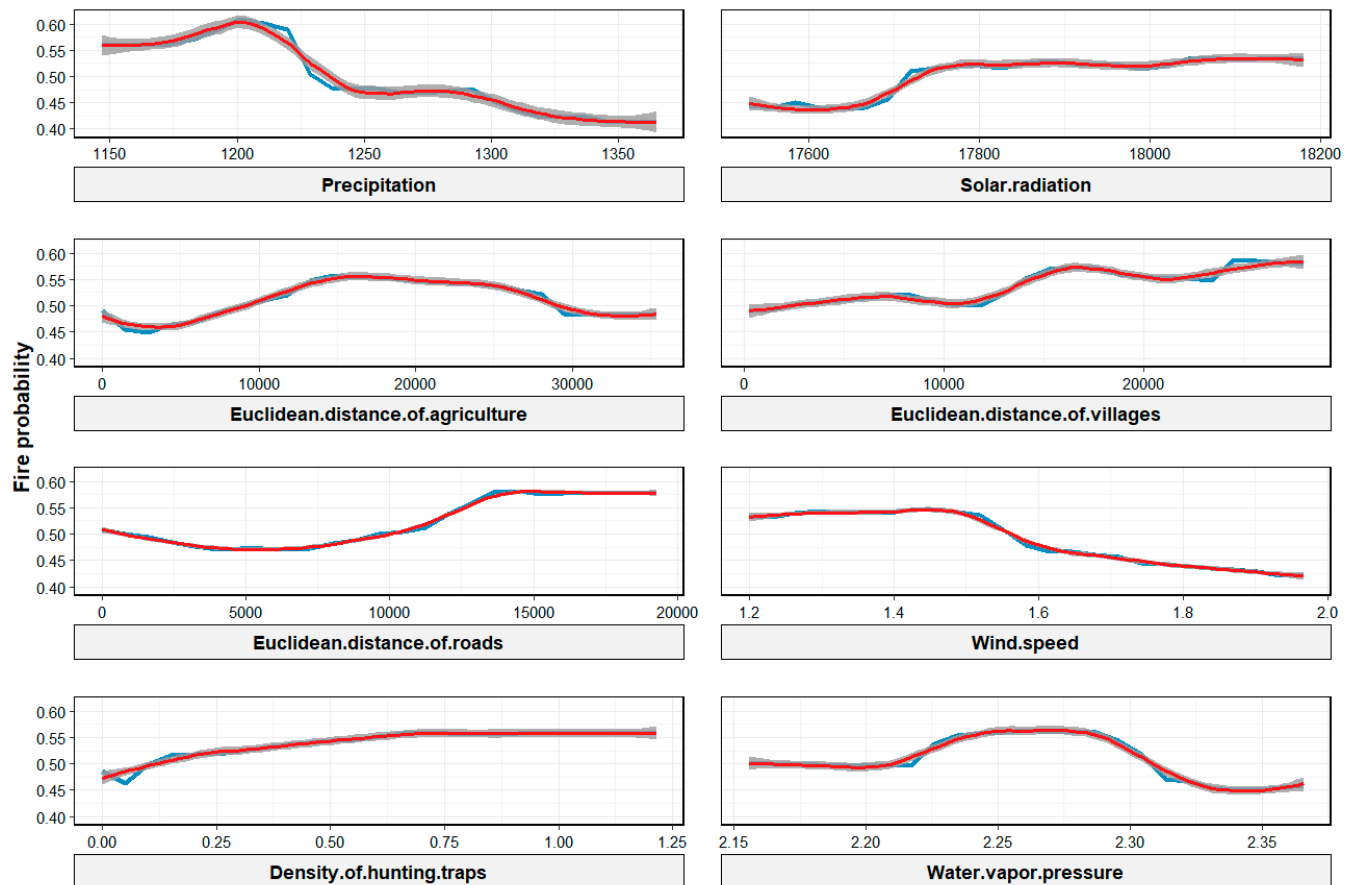


**Figure 8.** Partial dependence plots for variables that predict the occurrence of fires, selected using Random Forests Algorithm.

### 3.2.2. Modelling Fire Risk

Figure 9 illustrates the spatial distribution of fire risk in the PNAG, indicating that most of the areas of high and very high risk of fires are in the central region, especially nearby the ranger camps of Nassere, Etaga and Lice. According to field observations, very low to medium fire probability was associated with dominance of dense forest, especially around the Mulela, south of Lice, west of Mujaiane, north and south of Namurrua to the west of Nakololo and in some areas in the central region of the park. Areas with higher fire risk, are usually dominated by herbaceous vegetation and open forest in the interior of the park, and by agricultural activities in the buffer zone.

Table 7 shows that 15% of the total area of the park had very low fire risk, 17% had low risk, 11% medium risk, 13% medium-high risk, while around 43% experienced a higher probability of fire ignition. These areas experienced also higher density, intensity and frequency of fires.

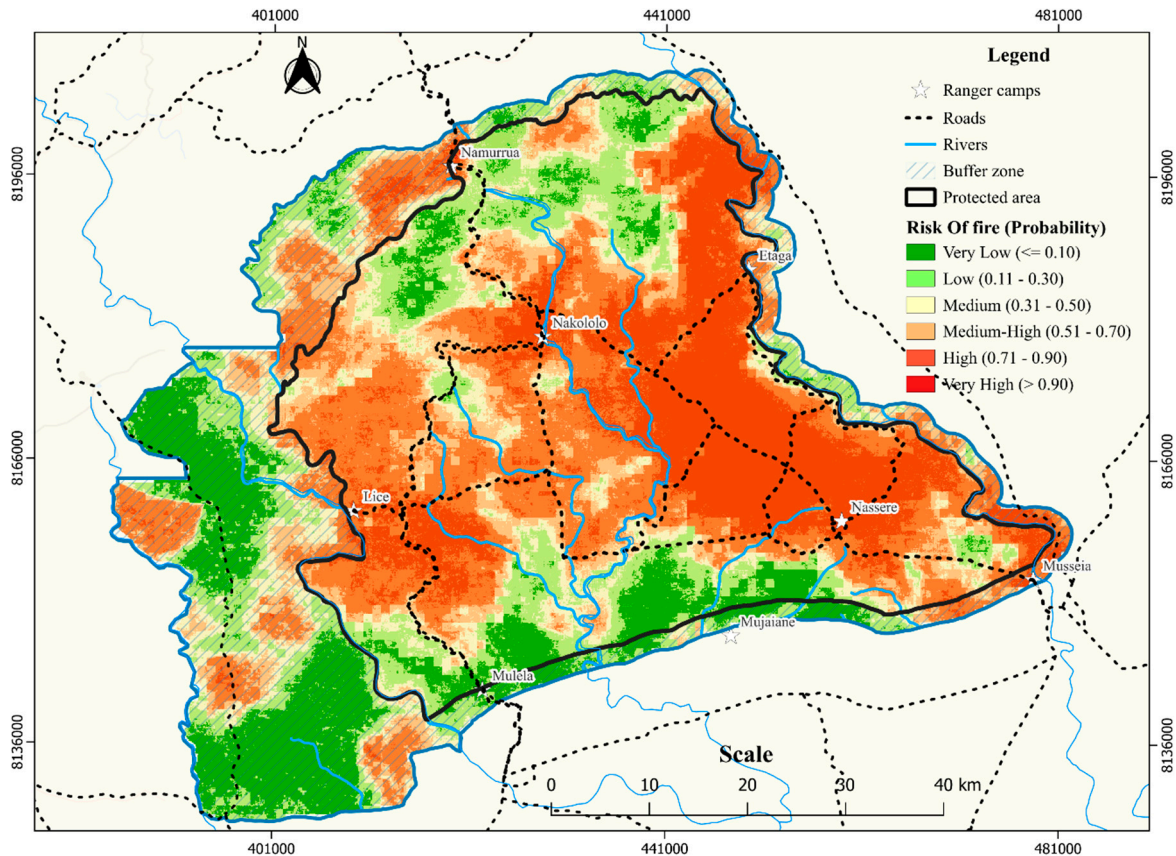


**Figure 9.** Spatial distribution of fire risk (likelihood of fire) in the Gilé National Park, explained by precipitation, solar radiation, water vapor deficit, wind speed, distance from agriculture fields, distance from settlements, distance from roads and density of hunting traps. .

**Table 5.** Area occupied by each class of fire risk (Likelihood of fire).

Likelihood of fire (fire risk)	Area (km <sup>2</sup> )	% of the total area
N/A (No data/no fire)	67.97	2
Very low (0-0.10)	633.37	15
Low (0.11-0.30)	748.02	17
Medium (0.31-0.50)	466.57	11
Medium to High (0.51-0.70)	561.53	13
High (0.71-0.90)	1081.90	25
Very High (0.91-1.00)	807.65	18
Total	4367	100

### 3.2.3. Accuracy Analysis and Kappa Index

The Kappa index (K) corresponded to an 80% degree of agreement, meaning that the model presents good classification quality. In terms of overall accuracy, there is approximately a 90.01% probability that the burned area corresponded to the truth found in the reference map, with 9% of the pixels at risk being wrongly classified as having low burning area.

## 4. Discussion

We conducted a comprehensive 23-year (2001-2023) assessment of fire regime dynamics in PNAG, central Mozambique, characterizing frequency, seasonality, intensity, density, and severity while modeling spatial risk patterns. Our findings demonstrate fire as a pervasive ecological driver, with mean recurrence intervals of 3.9 years. This aggregate metric, however, obscures critical spatial heterogeneity: the overwhelming majority (88%) of the park experiences annual or biennial burning. Such short intervals fall outside the 3-4 year window considered essential for maintaining functional Miombo ecosystem processes (Frost, 1996; Furley et al., 2008). When contextualized within regional literature, PNAG emerges as an outlier characterized by exceptionally high fire frequency. Regional studies typically document MFRI values of 3-5 years (Frost, 1996; Ribeiro et al., 2017; Wood et al., 2022) positioning PNAG at the intensive extreme of the spectrum. Additionally, Pungulanhe, (2020) recorded a mean return interval of 5.38 years in PNAG, suggesting that burning regimes have intensified in recent years. Such high recurrence rates demand urgent attention.

Short return intervals of 1-2 years may carry substantial ecological implications. Empirical evidence (Ryan and Williams, 2011; Magadzire, 2013; Salimo et al., 2025) indicates such intensive regimes systematically advantage herbaceous vegetation while suppressing woody recruitment. This creates a demographic bottleneck wherein saplings remain arrested in vulnerable size classes, progressively eroding woodland regeneration potential. With merely 7% of PNAG experiencing return intervals within the functional 3-4 year range, woodland recovery appears systemically compromised. Persistent fire pressure may progressively diminish biodiversity, carbon sequestration capacity, and adaptive resilience to climatic shifts, while elevating degradation risk and undermining ecosystem service provisioning over decadal timescales. These ecological relationships are addressed in another yet to come publication.

Our spatial analysis yielded counterintuitive results: fire frequency peaked within the core protection zone rather than in human-dominated buffer areas. This pattern diverges from findings in Burkina Faso and South Africa, where ignition density correlates positively with proximity to settlements and agricultural landscapes (Hudak and Brockett, 2004; Devineau, Fournier and Nignan, 2010). Several mechanisms may explain PNAG's atypical spatial signature: (i) hunting-associated ignitions, evidenced by elevated trap density within protected boundaries; (ii) fire use during honey harvesting operations; or (iii) biomass accumulation in less-disturbed interior zones creating high fuel loads. These results highlight the complexity of human–fire interactions in protected Miombo. Another plausible factor is the role of park ranger camps, where fire may be used (or accidentally triggered) for visibility, protection, or accessibility. In fact, we found that around the ranger camps all fire regime components stood out.

Temporal patterns demonstrated pronounced late dry-season concentration (August–October), consistent with regional Miombo fire climatology (Pereira et al., 2004; Ribeiro et al., 2017; Meneses et al., 2025). Peak intensity occurred as herbaceous fuels reached maximum curing, generating Fire Radiative Power exceeding 800 MW. High fire intensity in the central and northern zones, coupled with high recurrence, may accelerate transitions from woodland to grassland-dominated states (Van Langevelde et al., 2003). These conditions may threaten the long-term ecological integrity of PNAG.

Risk modeling revealed complex interactions between climatic drivers (precipitation regimes, solar radiation intensity, wind dynamics) and anthropogenic factors (hunting infrastructure density, agricultural proximity). Notably, ignition probability exhibited positive correlation with distance from settlements and cultivation zones, implying that fire origins relate more strongly to intra-park activities than to agricultural land-clearing. This underscores the importance of integrating socio-ecological monitoring (e.g., hunting activity) with remote sensing for effective fire governance.

Our findings provide an empirical basis for spatially differentiated management interventions (Supplementary Figure S1). Given high-risk concentration in central-eastern sectors, we recommend: (i) strategic early-season prescribed burning to mitigate late-season fire intensity; (ii) enhanced law enforcement, targeting hunting-associated ignitions; and (iii) collaborative fire governance engaging

buffer zone communities. Without intervention, the persistence of (bi) annual fire regimes may compromise PNAG's ability to maintain biodiversity, store carbon, and provide ecosystem services. Our findings therefore emphasize the urgency of implementing targeted fire management strategies to safeguard the ecological resilience and conservation value of PNAG.

## 5. Conclusions

Our multi-decadal analysis demonstrates that PNAG experiences fire recurrence patterns fundamentally incompatible with Miombo ecosystem resilience, as the dominant annual burning cycle substantially exceeds functional thresholds. This intensive regime poses systemic threats to biodiversity maintenance, carbon storage capacity, and ecosystem service delivery, potentially undermining both conservation objectives and community welfare. By identifying the climatic and anthropogenic drivers of fire risk, our findings provide a foundation for targeted interventions, including zoning for management priority, community fire management, and adaptive prescribed burning. Locally, these actions are essential to safeguard PNAG's ecological integrity and socio-economic value. Regionally and globally, the case of PNAG highlights how Miombo woodlands—a biome spanning 1.9 million km<sup>2</sup> and central to African livelihoods and global carbon balance—are increasingly vulnerable to recurrent fire. Protecting PNAG is therefore not only a national conservation priority but also a contribution to global commitments on biodiversity, climate mitigation, and sustainable development.

**Supplementary Materials:** The following supporting information can be downloaded at the website of this paper posted on Preprint.org. Figure S1.

**Funding:** Biofund Project number REF N°5/BIOFUND/SUB/PROMOVE/21. FCT—Fundação para a Ciência e Tecnologia, I.P. through project reference UID/00239/2025 (Forest Research Centre), PLCM—Programa de Liderança para a Conservação de Moçambique and Associate Laboratory TERRA (LA/P/0092/2020).

**Acknowledgments:** The authors would like to thank all the individuals who made this study possible, namely: Mr. Jone Fernando, Mrs. Ismenia Amaral, Mr. Macamo, Mr. Hermenegildo Mandlate, Mrs. Joana Govene. We also thank the institutional support of the Eduardo Mondlane University and the National Administration of Conservation Areas (ANAC) through the PNAG administrative team and Mr. Alessandro Fusari for his valuable contribution to fit the study into the management objectives of the park.

**Conflicts of Interest:** The authors declare no conflict of interest.

## References

1. Administração Nacional das Áreas de Conservação (ANAC, IP). (2024). Plano de Maneio do Parque Nacional do Gile 2024—2033 Versao Final.
2. Ameja, L. G., Ribeiro, N., Siteo, A. A., & Guillot, B. (2022). Regeneration and Restoration Status of Miombo Woodland Following Land Use Land Cover Changes at the Buffer Zone of Gile National Park, Central Mozambique. *Trees, Forests and People*, 9, 100290. <https://doi.org/10.1016/j.tfp.2022.100290>
3. Andela, N., Morton, D. C., Giglio, L., Chen, Y., Van Der Werf, G. R., Kasibhatla, P. S., DeFries, R. S., Collatz, G. J., Hantson, S., Kloster, S., Bachelet, D., Forrest, M., Lasslop, G., Li, F., Mangeon, S., Melton, J. R., Yue, C., & Randerson, J. T. (2017). A human-driven decline in global burned area. *Science*, 356(6345), 1356–1362. <https://doi.org/10.1126/science.aal4108>
4. Aquino, A., Lim, C., Kaechele, K., & Taquidir, M. (2018). Mozambique Country Forest Note.
5. Aragão, L. E. O. C., Malhi, Y., Barbier, N., Lima, A., Shimabukuro, Y., Anderson, L., & Saatchi, S. (2008). Interactions between rainfall, deforestation and fires during recent years in the Brazilian Amazonia. *Philosophical Transactions of the Royal Society B: Biological Sciences*, 363(1498), 1779–1785. <https://doi.org/10.1098/rstb.2007.0026>

6. Archibald, S., Roy, D. P., Van Wilgen, B. W., & Scholes, R. J. (2009). What limits fire? An examination of drivers of burnt area in Southern Africa. *Global Change Biology*, 15(3), 613–630. <https://doi.org/10.1111/j.1365-2486.2008.01754.x>
7. Assédé, E. S. P., Azihou, A. F., Geldenhuys, C. J., Chirwa, P. W., & Biaou, S. S. H. (2020). Sudanian versus Zambezian woodlands of Africa: Composition, ecology, biogeography and use. *Acta Oecologica*, 107, 103599. <https://doi.org/10.1016/j.actao.2020.103599>
8. Bond, W., & Keeley, J. (2005). Fire as a global ‘herbivore’: The ecology and evolution of flammable ecosystems. *Trends in Ecology & Evolution*, 20(7), 387–394. <https://doi.org/10.1016/j.tree.2005.04.025>
9. Breiman, L. (2001). Random Forests. *Machine Learning*, 45(1), 5–32. <https://doi.org/10.1023/A:1010933404324>
10. Buramuge, V. A., Ribeiro, N. S., Olsson, L., Bandeira, R. R., & Lisboa, S. N. (2023). Tree Species Composition and Diversity in Fire-Affected Areas of Miombo Woodlands, Central Mozambique. *Fire*, 6(1), 26. <https://doi.org/10.3390/fire6010026>
11. Campbell, B. M., Campbell, B., & Center for International Forestry Research (Eds.). (1996). *The miombo in transition: Woodlands and welfare in Africa*. Center for International Forestry Research.
12. Chuvieco, E., Mouillot, F., Van Der Werf, G. R., San Miguel, J., Tanase, M., Koutsias, N., García, M., Yebra, M., Padilla, M., Gitas, I., Heil, A., Hawbaker, T. J., & Giglio, L. (2019). Historical background and current developments for mapping burned area from satellite Earth observation. *Remote Sensing of Environment*, 225, 45–64. <https://doi.org/10.1016/j.rse.2019.02.013>
13. Conedera, M., Tinner, W., Neff, C., Meurer, M., Dickens, A. F., & Krebs, P. (2009). Reconstructing past fire regimes: Methods, applications, and relevance to fire management and conservation. *Quaternary Science Reviews*, 28(5–6), 555–576. <https://doi.org/10.1016/j.quascirev.2008.11.005>
14. Devineau, J.-L., Fournier, A., & Nignan, S. (2010). Savanna fire regimes assessment with MODIS fire data: Their relationship to land cover and plant species distribution in western Burkina Faso (West Africa). *Journal of Arid Environments*, 74(9), 1092–1101. <https://doi.org/10.1016/j.jaridenv.2010.03.009>
15. Dewees, P. A., Campbell, B. M., Katerere, Y., Siteo, A., Cunningham, A. B., Angelsen, A., & Wunder, S. (2011). Managing the Miombo Woodlands of Southern Africa: Policies, Incentives and Options for the Rural Poor. *Journal of Natural Resources Policy Research*, 2(1), 57–73. <https://doi.org/10.1080/19390450903350846>
16. Dziba, L., Ramoelo, A., Ryan, C., Harrison, S., Pritchard, R., Tripathi, H., Sitas, N., Selomane, O., Engelbrecht, F., Pereira, L., Katerere, Y., Chirwa, P. W., Ribeiro, N. S., & Grundy, I. M. (2020). Scenarios for Just and Sustainable Futures in the Miombo Woodlands. In N. S. Ribeiro, Y.
17. Katerere, P. W., Chirwa, & I. M. Grundy (Eds.), *Miombo Woodlands in a Changing Environment: Securing the Resilience and Sustainability of People and Woodlands* (pp. 191–234). Springer International Publishing. <https://doi.org/10.1007/978-3-030-50104-46>
18. Etc Terra. (2017). Project Design Document of GNR REDD Project. Validated by VCS. (No. 3; JOINT PROJECT DESCRIPTION & MONITORING REPORT: VCS Version 3).
19. Frost, P. G. H. (1996). The ecology of miombo woodlands. In B. Campbell (Ed.), *The Miombo in Transition: Woodlands and Welfare in Africa*.
20. Frost, P. G. H., & Robertson, F. (1987). *The Ecological Effects of Fire in Savannas*.
21. Furley, P. A., Rees, R. M., Ryan, C. M., & Saiz, G. (2008). Savanna burning and the assessment of long-term fire experiments with particular reference to Zimbabwe. *Progress in Physical Geography: Earth and Environment*, 32(6), 611–634. <https://doi.org/10.1177/0309133308101383>
22. Gandiwa, E. (2011). Effects of repeated burning on woody vegetation structure and composition in a semi-arid southern African savanna. 2.
23. Giglio, L., Descloitres, J., Justice, C. O., & Kaufman, Y. J. (2003). An Enhanced Contextual Fire Detection Algorithm for MODIS. *Remote Sensing of Environment*, 87(2–3), 273–282. [https://doi.org/10.1016/S0034-4257\(03\)00184-6](https://doi.org/10.1016/S0034-4257(03)00184-6)
24. Giglio, L., Randerson, J. T., & Van Der Werf, G. R. (2013). Analysis of daily, monthly, and annual burned area using the fourth-generation global fire emissions database (GFED4). *Journal of Geophysical Research: Biogeosciences*, 118(1), 317–328. <https://doi.org/10.1002/jgrg.20042>

25. Giglio, L., Schroeder, W., Hall, J. V., & Justice, C. O. (2018). MODIS Collection 6 Active Fire Product User's Guide Revision B.
26. Giglio, L., Schroeder, W., & Justice, C. O. (2016). The collection 6 MODIS active fire detection algorithm and fire products. *Remote Sensing of Environment*, 178, 31–41. <https://doi.org/10.1016/j.rse.2016.02.054>
27. Gonçalves, Y. L. M., Siqueira, E. S., Ferreira, C. A., Teixeira, M. D. S., Correa, P. D. V., & Urbinati, C. V. (2022). Aplicação de algoritmos de Random Forest no suporte à identificação das espécies *Handroanthus Serratifolius* (Vahl) S. O. Grose e *Handroanthus Impetiginosus* (Mart. Ex DC.) Mattos (bignoniaceae). *Brazilian Journal of Development*, 8(5), 39721–39735. <https://doi.org/10.34117/bjdv8n5-457>
28. Goryl, P., Buongiorno, A., Santella, C., Fournier-Sicre, V., & Santacesaria, V. (2012). Active fire: fire detection and fire radiative power assessment.
29. Govender, N., Trollope, W. S. W., & Van Wilgen, B. W. (2006). The effect of fire season, fire frequency, rainfall and management on fire intensity in savanna vegetation in South Africa. *Journal of Applied Ecology*, 43(4), 748–758. <https://doi.org/10.1111/j.13652664.2006.01184.x>
30. He, T., Lamont, B. B., & Pausas, J. G. (2019). Fire as a key driver of Earth's biodiversity. *Biological Reviews*, 94(6), 1983–2010. <https://doi.org/10.1111/brv.12544>
31. Hijmans, R. J. (2025). raster: Geographic Data Analysis and Modeling. <https://github.com/rs/raster>
32. Hudak, A. T., & Brockett, B. H. (2004). Mapping fire scars in a southern African savannah using Landsat imagery. *International Journal of Remote Sensing*, 25(16), 3231–3243. <https://doi.org/10.1080/01431160310001632666>
33. Huntington, J. L., Hegewisch, K. C., Daudert, B., Morton, C. G., Abatzoglou, J. T., McEvoy, D. J., & Erickson, T. (2017). Climate Engine: Cloud Computing and Visualization of Climate and Remote Sensing Data for Advanced Natural Resource Monitoring and Process Understanding. *Bulletin of the American Meteorological Society*, 98(11), 2397–2410. <https://doi.org/10.1175/BAMS-D-15-00324.1>
34. Keeley, J. E. (2009). Fire intensity, fire severity and burn severity: A brief review and suggested usage. *International Journal of Wildland Fire*, 18(1), 116. <https://doi.org/10.1071/WF07049>.
35. Key, C. H., & Benson, N. C. (2006). Landscape Assessment: Ground measure of severity, the Composite Burn Index; and Remote sensing of severity, the Normalized Burn Ratio.
36. Konkathi, P., & Shetty, A. (2021). Inter comparison of post-fire burn severity indices of Landsat-8 and Sentinel-2 imagery using Google Earth Engine. *Earth Science Informatics*, 14(2), 645–653. <https://doi.org/10.1007/s12145-020-00566-2>.
37. Koproski, L., Ferreira, M. P., Goldammer, J. G., & Batista, A. C. (2011). Modelo de zoneamento de risco de incêndios para unidades de conservação brasileiras: O Caso do Parque Estadual Do Cerrado (Pr). *Floresta*, 41(3). <https://doi.org/10.5380/rf.v41i3.24049>
38. Krebs, P., Pezzatti, G. B., Mazzoleni, S., Talbot, L. M., & Conedera, M. (2010). Fire regime: History and definition of a key concept in disturbance ecology. *Theory in Biosciences*, 129(1), 53–69. <https://doi.org/10.1007/s12064-010-0082-z>.
39. Liaw, A., & Wiener, M. (2002). Classification and Regression by randomForest. 2.
40. Lutes, D. C., Keane, R. E., Caratti, J. F., Key, C. H., Benson, N. C., Sutherland, S., & Gangi, L. J. (2006). FIREMON: Fire effects monitoring and inventory system (No. RMRS-GTR-164; p. RMRS-GTR-164). U.S. Department of Agriculture, Forest Service, Rocky Mountain Research Station. <https://doi.org/10.2737/RMRS-GTR-164>
41. Macave, O. A., Ribeiro, N. S., Ribeiro, A. I., Chauque, A., Bandeira, R., Branquinho, C., & Washington-Allen, R. (2022). Modelling Aboveground Biomass of Miombo Woodlands in Niassa Special Reserve, Northern Mozambique. *Forests*, 13(2), 311. <https://doi.org/10.3390/f13020311>
42. Magadzire, N. (2013). Reconstruction of a fire regime using MODIS burned area data: Charara Safari Area, Zimbabwe [Thesis, Stellenbosch University]. <http://scholar.sun.ac.za>
43. Magalhães, T. M. (2025). What is left in miombo woodlands? Rarity and commonness of woody species, commercial timber species, and lawful harvestable diameter classes. *Heliyon*, 11(2), e41821. <https://doi.org/10.1016/j.heliyon.2025.e41821>

44. Meneses, O. M., Ribeiro, N. S., Shirvani, Z., & Andrew, S. M. (2024). Spatio-Temporal Analysis of Wildfire Regimes in Miombo of the LevasFlor Forest Concession, Central Mozambique. *Fire*, 7(8), 264. <https://doi.org/10.3390/fire7080264>
45. Meneses, O. M., Ribeiro, N. S., Shirvani, Z., & Andrew, S. M. (2025). Resilience of the Miombo Woodland to Different Fire Frequencies in the LevasFlor Forest Concession, Central Mozambique. *Forests*, 16(1), 10. <https://doi.org/10.3390/f16010010>
46. Mercier, C., Grinand, C., Randrianary, T., Nourtier, M., & Rabany, C. (2016). Background study for the preparation of the Zambézia Integrated Landscapes Management Program [Report for Government of Mozambique and FCPF.]. Etc Terra e Rongead.
47. Milà, C., Ludwig, M., Pebesma, E., Tonne, C., & Meyer, H. (2024). Random forests with spatial proxies for environmental modelling: Opportunities and pitfalls [Preprint]. *Earth and space science informatics*. <https://doi.org/10.5194/egusphere-2024-138>
48. Miombo Network. (2016). Using & restoring the Miombo woodlands: Needs for an integrated and holistic approach in ecosystem management for long term sustainability. 5203881 Bytes. <https://doi.org/10.6084/M9.FIGSHARE.99889>
49. Montfort, F. (2021). Dynamiques des paysages forestiers au Mozambique: Étude de l'écologie du Miombo pour contribuer aux stratégies de restauration des terres dégradées. *BOIS & FORETS DES TROPIQUES*, 357, 105–106. <https://doi.org/10.19182/bft2023.357.a37281>
50. Montfort, F., Nourtier, M., Grinand, C., Maneau, S., Mercier, C., Roelens, J.-B., & Blanc, L. (2021). Regeneration capacities of woody species biodiversity and soil properties in Miombo woodland after slash-and-burn agriculture in Mozambique. *Forest Ecology and Management*, 488, 119039. <https://doi.org/10.1016/j.foreco.2021.119039>
51. Novo, A., Fariñas-Álvarez, N., Martínez-Sánchez, J., González-Jorge, H., Fernández-Alonso, J. M., & Lorenzo, H. (2020). Mapping Forest Fire Risk—A Case Study in Galicia (Spain). *Remote Sensing*, 12(22), 3705. <https://doi.org/10.3390/rs12223705>
52. Pausas, J. G., & Keeley, J. E. (2009). A Burning Story: The Role of Fire in the History of Life. *BioScience*, 59(7), 593–601. <https://doi.org/10.1525/bio.2009.59.7.10>
53. Pereira, J. M. C., Mota, B., Privette, J. L., Caylor, K. K., Silva, J. M. N., Sá, A. C. L., & Ni-Meister, W. (2004). A simulation analysis of the detectability of understory burns in miombo woodlands. *Remote Sensing of Environment*, 93(3), 296–310. <https://doi.org/10.1016/j.rse.2004.01.009>
54. Pungulanhe, L. A. (2020). Caracterização da vegetação arbórea sob diferentes regimes de queimadas na floresta de miombo, reserva nacional do Gilé [Dissertação apresentada à Faculdade de Agronomia e Engenharia Florestal/UEM, como parte dos requisitos para obtenção do título de Mestre em Maneio e Conservação da Biodiversidade.]. Universidade Eduardo Mondlane.
55. QGIS Development Team. (2024). QGIS Geographic Information System (Version 3.40) [Computer software]. <https://www.qgis.org/en/site/>
56. R Core Team. (2023). R: A Language and Environment for Statistical Computing [Computer software]. <https://www.R-project.org/>
57. Ribeiro, N., Nazerali, S., & Chauque, A. (2020). A contribution to Mozambique's biodiversity offsetting system: Framework to assess the ecological condition of Miombo Woodlands.
58. Ribeiro, N. S., Cangela, A., Chauque, A., Bandeira, R. R., & Ribeiro-Barros, A. I. (2017). Characterisation of spatial and temporal distribution of the fire regime in Niassa National Reserve, northern Mozambique. *International Journal of Wildland Fire*, 26(12), 1021. <https://doi.org/10.1071/WF17085>
59. Ribeiro, N. S., Matos, C. N., Moura, I. R., Washington-Allen, R. A., & Ribeiro, A. I. (2013). Monitoring vegetation dynamics and carbon stock density in miombo woodlands. *Carbon Balance and Management*, 8(1), 11. <https://doi.org/10.1186/1750-0680-8-11>
60. Ribeiro, N. S., Shugart, H. H., Swap, R. J., & Okin, G. S. (2007). Five-year period of fire regime in the Miombo Woodlands of Niassa Reserve, Mozambique in northern Mozambique [PhD Thesis]. University of Virginia.
61. Ribeiro, N. S., Shugart, H. H., & Washington-Allen, R. (2008). The effects of fire and elephants on species composition and structure of the Niassa Reserve, northern Mozambique. *Forest Ecology and Management*, 255(5–6), 1626–1636. <https://doi.org/10.1016/j.foreco.2007.11.033>

62. Roy, D. P., Boschetti, L., Justice, C. O., & Ju, J. (2008). The collection 5 MODIS burned area product—Global evaluation by comparison with the MODIS active fire product. *Remote Sensing of Environment*, 112(9), 3690–3707. <https://doi.org/10.1016/j.rse.2008.05.013>
63. Running, S., Mu, Q., & Zhao, M. (2017). MOD16A2 MODIS/Terra Net Evapotranspiration 8-Day L4 Global 500m SIN Grid V006 [Dataset]. NASA Land Processes Distributed Active Archive Center. <https://doi.org/10.5067/MODIS/MOD16A2.006>
64. Ryan, C. M., Pritchard, R., McNicol, I., Owen, M., Fisher, J. A., & Lehmann, C. (2016). Ecosystem services from southern African woodlands and their future under global change. *Philosophical Transactions of the Royal Society B: Biological Sciences*, 371(1703), 20150312. <https://doi.org/10.1098/rstb.2015.0312>
65. Ryan, C. M., & Williams, M. (2011). How does fire intensity and frequency affect miombo woodland tree populations and biomass? *Ecological Applications*, 21, 48–60. <https://doi.org/10.1890/09-1489.1>
66. Salimo, M., Buramuge, V., Farão, A., Chauque, A., Bandeira, R., Fernando, J., Ribeiro-Barros, A. I., Branquinho, C., & Ribeiro, N. (2025). Insights on the dynamics of Miombo woody vegetation in Niassa Special Reserve, northern Mozambique. *International Journal of Wildland Fire*, 34(5). <https://doi.org/10.1071/WF24060>
67. Schroeder, W., Prins, E., Giglio, L., Csaszar, I., Schmidt, C., Morisette, J., & Morton, D. (2008). Validation of GOES and MODIS active fire detection products using ASTER and ETM+ data. *Remote Sensing of Environment*, 112(5), 2711–2726. <https://doi.org/10.1016/j.rse.2008.01.005>
68. Silva, I. S., Garcia, C. A. B., Alves, P. H., & Garcia, H. L. (2019). Aplicação do Algoritmo Random Forest na Avaliação de Corpos Hídricos no Estado de Sergipe.
69. Silva, J. M. N., Sá, A. C. L., & Pereira, J. M. C. (2005). Comparison of burned area estimates derived from SPOT-VEGETATION and Landsat ETM+ data in Africa: Influence of spatial pattern and vegetation type. *Remote Sensing of Environment*, 96(2), 188–201. <https://doi.org/10.1016/j.rse.2005.02.004>
70. Silva Junior, C. H. L., Aragão, L. E. O. C., Fonseca, M. G., Almeida, C. T., Vedovato, L. B., & Anderson, L. O. (2018). Deforestation-Induced Fragmentation Increases Forest Fire Occurrence in Central Brazilian Amazonia. *Forests*, 9(6), 305. <https://doi.org/10.3390/f9060305>
71. Soriano, B. M. A., Daniel, O., & Santos, S. A. (2015). Eficiência de índices de risco de incêndios para o Pantanal Sul-Mato-Grossense. *Ciência Florestal*, 25(4), 809–816. <https://doi.org/10.5902/1980509820231>
72. Tiecke, T. G., Liu, X., Zhang, A., Gros, A., Li, N., Yetman, G., Kilic, T., Murray, S., Blankespoor, B., Prydz, E. B., & Dang, H.-A. H. (2017). Mapping the World Population One Building at a Time. World Bank, Washington, DC. <https://doi.org/10.1596/33700>
73. Torres, F. T. P., Ribeiro, G. A., Martins, S. V., & Lima, G. S. (2011). Correlações entre os elementos meteorológicos e as ocorrências de incêndios florestais na área urbana de Juiz de Fora, MG. *Revista Árvore*, 35(1), 143–150. <https://doi.org/10.1590/S0100-67622011000100017>
74. UN-SPIDER (United Nations Platform for Space-based Information for Disaster Management and Emergency Response). (2023). Recommended Practice: Burn Severity Mapping. Step-by-Step: Burn Severity in Google Earth Engine. Retrieved from <https://www.un-spider.org/advisory-support/recommended-practices/recommended-practice-burnseverity/step-by-step/burn-severity-google-earth-engine>.
75. Vallejo-Villalta, I., Rodríguez-Navas, E., & Márquez-Pérez, J. (2019). Mapping Forest Fire Risk at a Local Scale—A Case Study in Andalusia (Spain). *Environments*, 6(3), 30. <https://doi.org/10.3390/environments6030030>
76. Van Langevelde, F., Van De Vijver, C. A. D. M., Kumar, L., Van De Koppel, J., De Ridder, N., Van Andel, J., Skidmore, A. K., Hearne, J. W., Stroosnijder, L., Bond, W. J., Prins, H. H. T., & Rietkerk, M. (2003). EFFECTS OF FIRE AND HERBIVORY ON THE STABILITY OF SAVANNA ECOSYSTEMS. *Ecology*, 84(2), 337–350. [https://doi.org/10.1890/0012-9658\(2003\)084\[0337:EOFAHO\]2.0.CO;2](https://doi.org/10.1890/0012-9658(2003)084[0337:EOFAHO]2.0.CO;2)
77. Whitlock, C., Higuera, P. E., McWethy, D. B., & Briles, C. E. (2010). Paleocological Perspectives on Fire Ecology: Revisiting the Fire-Regime Concept.
78. Wood, E., Mgaya, M., Andrews, C., Schreckenber, K., Fisher, J. A., Grundy, I., & Ryan, C. M. (2022). Intentions behind common and risky fires in south-eastern Tanzania. *African Journal of Range & Forage Science*, 39(1), 124–135. <https://doi.org/10.2989/10220119.2021.2000026>

79. Wooster, M. J., Roberts, G., Perry, G. L. W., & Kaufman, Y. J. (2005). Retrieval of biomass combustion rates and totals from fire radiative power observations: FRP derivation and calibration relationships between biomass consumption and fire radiative energy release. *Journal of Geophysical Research: Atmospheres*, 110(D24), 2005JD006318. <https://doi.org/10.1029/2005JD006318>

**Disclaimer/Publisher's Note:** The statements, opinions and data contained in all publications are solely those of the individual author(s) and contributor(s) and not of MDPI and/or the editor(s). MDPI and/or the editor(s) disclaim responsibility for any injury to people or property resulting from any ideas, methods, instructions or products referred to in the content.